Mathematical Geology, Vol. 38, No. 5, July 2006 (© 2006)
DOI: 10.1007/s11004-006-9029-9

A Connectivity Index for Discrete Fracture Networks[1]

C. Xu,[2] P. A. Dowd,[3] K. V. Mardia,[4] and R. J. Fowell[5]

Connectivity is an important measure for assessing flow transport in rock, especially through fractures. In this paper, rock fracture systems are modelled by a discrete fracture model simulated by a marked point process. A connectivity index is then introduced to quantify the connectivity between any two points in space. Monte Carlo simulation is used to evaluate the connectivity index for stationary cases and relationships between the connectivity index and the parameters of the discrete fracture model are analysed. The average number of intersections per fracture, X_f, and the fracture intensity, P12 *(*P32*), are calculated and the relationships between these parameters and the connectivity index are investigated, concluding that X_f is the more suitable parameter for the classification of rock mass flow properties. The relationships between the connectivity index and the percolation state of the fractured medium are also discussed. An edge correction is briefly discussed and a practical example is used to demonstrate the method of computing the connectivity index.*

KEY WORDS: connectivity index, marked point process, discrete fracture model, rock fracture system, rock mass flow property classification, percolation.

INTRODUCTION

In evaluating the suitability of underground sites for the disposal or storage of hazardous wastes, it is important to assess the uncertainty associated with possible pollutant trajectories from the repository. In general, volcanic rocks provide the most suitable repositories (SKB, 2003; Yucca Mountain, 2004) and flow behaviours in these rocks are fundamentally different to those encountered in other applications such as hydrocarbon reservoirs in which flows through permeable porous media are of primary interest (Deutsch, 2002; Long and others,

[1]Received 15 November 2004; accepted 13 January 2006; Published online: 7 November 2006.
[2]Department of Mining and Mineral Engineering, University of Leeds, Leeds, LS2 9JT, UK; e-mail: c.xu@leeds.ac.uk
[3]Faculty of Engineering, Computer and Mathematical Sciences, University of Adelaide, SA 5005, Australia; e-mail: peter.dowd@adelaide.edu.au
[4]Department of Statistics, University of Leeds, Leeds, LS2 9JT, UK; e-mail: k.v.mardia@leeds.ac.uk
[5]Department of Mining and Mineral Engineering, University of Leeds, Leeds, LS2 9JT, UK; e-mail: r.j.fowell@leeds.ac.uk

1982). A common approach to the modelling and prediction of pollutant trajectories is to use discrete fracture models (DFM) in which flow can only occur around the fracture surfaces and the (un-fractured intact) rock is assumed to be impermeable (Dershowitz and others, 1999; Rhén and Smellie, 2003; NRC, 1996).

In the DFM approach, pollutants are transported or, in the case of closed fractures, dissipated, from a source to a destination point if a pathway can be found through the discrete fracture network connecting the destination to the source. Hence, an evaluation of the connectivity of any two points in the volume (area) is fundamental to the problem. Published work using DFM focuses either on the percolation of the whole region studied (see below) or on the mechanism of particle transport through the fracture network but ignores the connectivity *per se* (e.g., Outters, 2003). In most environmental applications the existence of a pathway (connection) between two points is more important than the length or route of the pathway or of the time it takes for a pollutant to traverse it. In addition, most of the fracture networks studied in these applications are far from the percolation state but an evaluation of connectivity is required so that the risk of pollutant transportation can be assessed.

Percolation theory is the conventional way of dealing with connectivity issues related to DFM (Robinson, 1983; Stauffer and Aharony, 1994; Sahimi, 1993). In general, this approach focuses on the connectivity of a region (a volume in 3D or an area in 2D) at a specific scale and investigates the fracture networks required for the region to reach the percolation state, at which there is a sudden change in the behaviour of flow transport "through" the region, i.e., from an impermeable to a permeable state when an "infinite" fracture cluster can be found in the system connecting the boundaries of the region so that the whole system is percolating. Thus, any conclusions reached in this approach are global (i.e., the region considered as a whole) and, in general, scale-dependent (except for exceptional cases when the fracture system is strictly fractal and homogeneous).

The connectivity index (CI) approach described here studies the same problem from a slightly different perspective. Given a fracture system (described by a fracture model, or a fracture network model, derived theoretically or from known data) within a region, which may, or may not, be at the percolation state, the CI is the probability that two arbitrary points within the region are connected. The CI is, therefore, local and independent of the scale of the region. The CI can, however, be used to evaluate the percolation thresholds when combined with percolation criteria and the scale of the system (see below).

The connectivity index for the DFM is based on the definition of Allard (1993) and fractures are modelled as marked point processes. Monte Carlo simulation is used to evaluate the connectivity index and to assess the influence on connectivity of different fracture network models.

CONNECTIVITY INDEX

Two points x and y within a region R (i.e., a volume V in 3D or an area A in 2D) are denoted by $x \leftrightarrow y$ if they are connected, i.e., if there exists a pathway through the fracture network that connects points x and y. A connectivity index (or function), denoted by $\tau(\cdot)$, is defined as the probability that the two points are connected, i.e.,

$$\tau(x, y) = P(x \leftrightarrow y), \quad \forall x, y \in R \tag{1}$$

Obviously $\tau(x, y) \equiv \tau(y, x)$. Note that x and y denote location vectors, which in the 2D case are (x_1, x_2) and (y_1, y_2) respectively where subscripts 1 and 2 represent the two reference axes used. This definition is based on the connectivity function defined by Allard (1993, 1994) for permeable reservoirs in petroleum applications. The original definition is conditional on the assumption that both points belong to the same permeable phase or permeable lithofacies. This condition is not imposed on the index described here as the interest is in the estimated unconditional probability of connection so as to provide a measure of the connectivity of the entire region.

Allard's definition is used in a geostatistical context in which each block is assigned a permeable or non-permeable phase and the connectivity network is constructed by examining the phases of neighbouring blocks. Different connectivity functions are therefore needed for different (subjective) definitions of neighbourhoods around blocks and/or for different block shapes. For a rectangular block, Allard (1993) define a 4-connectivity function for edge (line) connectivity and an 8-connectivity function for edge connectivity and vertex (corner) connectivity. Pardo-Igúzquiza and Dowd (2003) introduce 6-, 18- and 26-connectivity functions for three-dimensional blocks.

An objective approach is followed in this paper. The connectivity of two points is assessed solely on the basis of whether there is a pathway through the fracture network connecting the points and thus only one connectivity index (function) is defined. There is, however, a support problem associated with the definition given in Equation (1). Point values cause difficulties (as explained below) in calculating the function and so non-point values or, in the geostatistical terminology, non-point supports, are used to define the index. This revised definition is compatible with practical applications as flow and transport are usually modelled at the scale of a given support (e.g. grid blocks).

Assuming the smallest unit (the support) for the connectivity index evaluation is v, $x_v \leftrightarrow y_v$ signifies that support v, centred at x, and support v, centred at y, are connected, while $x_v \not\leftrightarrow y_v$ denotes that they are not connected. Two supports are connected if there exists a pathway, or pathways, through the fracture network that pass through (intersect) the two supports, as illustrated by a 2D example in

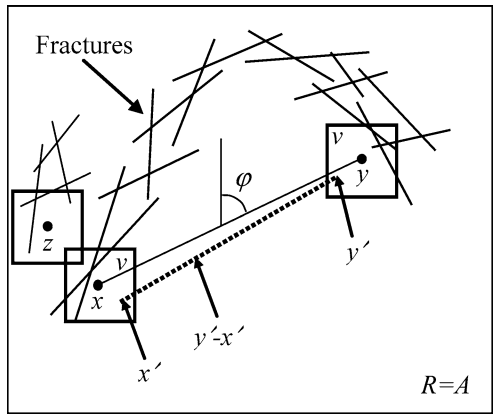

Figure 1. $\tau_v(x,y)$, $x_v \leftrightarrow y_v$ and $x_v \nleftrightarrow z_v$.

Figure 1. The connectivity index between x and y, based on support v, is then defined as:

$$\tau_v(x, y) = P(x_v \leftrightarrow y_v) \quad \forall x_v, y_v \in R \tag{2}$$

which is related to the point definition by:

$$\tau_v(x, y) = \int_v \int_v \tau(x', y') \cdot dx' \cdot dy' \tag{3}$$

where the integration is interpreted as the average of the point function $\tau(x', y')$ when x' and y' fully and independently describe the supports v_x and v_y (cf. Fig. 1).

Note that, although this definition is non-stationary in nature, its stationary counterpart may be more useful if the process controlling the fracture system (e.g., a marked point process) is considered stationary (see example below).

DISCRETE FRACTURE MODEL

Fracture networks play a key role in the evaluation of connectivity within the context discussed in this paper. Unlike permeable phases or lithofacies in petroleum engineering, fractures in general have a very small third dimension, the aperture. In volcanic formations, apertures are restricted to the range 100–500 μm (Priest, 1993), whereas they may be tens or hundreds of metres in length. Flow transport is only possible along the fracture surfaces and is restricted by any aperture-filling materials (Lee and Farmer, 1993).

For the reasons discussed above, the connectivity evaluations conducted by Allard (1993, 1994), using a truncated Gaussian and fixed primary grain Boolean

model, and by Pardo-Igúzquiza and Dowd (2003), using an indicator algorithm, are not considered suitable for the applications described here. Instead, the fracture random set is generated by a marked point process model.

Marked point processes are commonly used to model rare events such as fractures in crystalline rock (Lee, Veneziano, and Einstein, 1990; Stoyan, Kendall, and Mecke, 1995). The locations of fractures are modelled by a point process and the attributes (size, shape, orientation, aperture) of the fractures are modelled by marks associated with the point process. If the marks are generated independently, the fracture random set is equivalent to a Boolean model.

As a motivating practical two-dimensional example, Figure 2A shows a set of fracture traces on a rock outcrop taken from Hudson and Priest (1983). If we use the mid-point of the fractures (ignoring the truncation issue) to represent the locations of fractures we obtain the point dataset shown in Figure 2B. In this example, two marks are required for each point to represent the fracture, namely

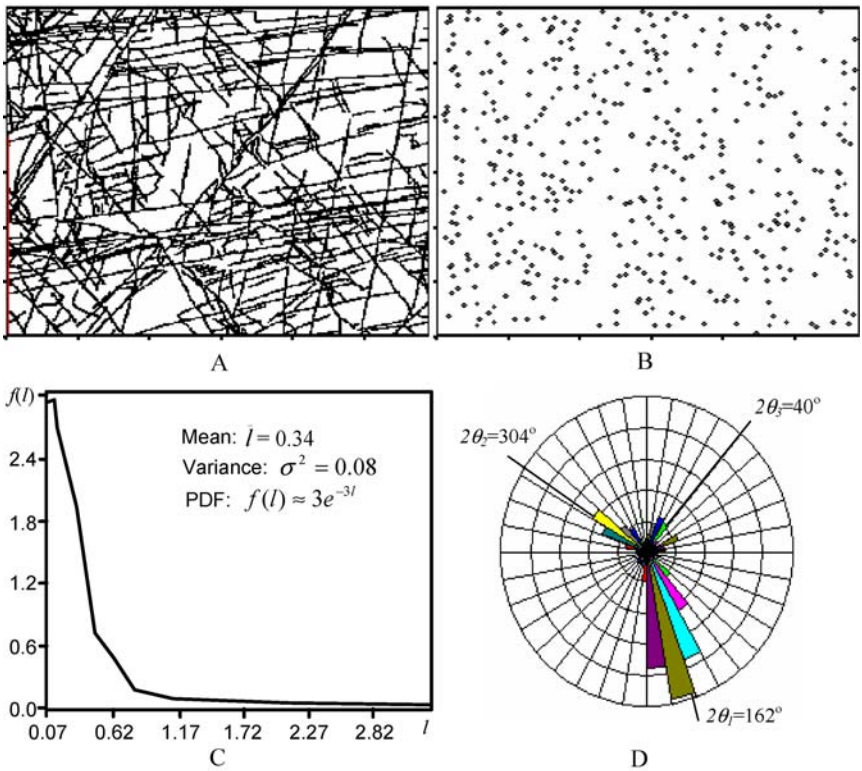

Figure 2. A, A set of fractures, B, Corresponding point dataset, C, Fracture length mark, *l*, and D, Rosegram of orientation mark (doubled azimuth angles).

length and orientation. The probability density function (pdf) of the length mark and the rose diagram for the orientation mark (double the azimuth angle) for this example are shown in Figures 2C and 2D respectively.

It is then possible to construct a point process model to represent the point pattern in Figure 2B, using common models such as homogeneous and non-homogeneous Poisson models, cluster models and Cox models. The goodness-of-fit of the models can be assessed from summary statistics such as the inter-event distance function $H(t)$, the nearest-event distance $G(t)$ or the K-function $K(t)$, see Diggle (2003), Cressie (1993) and Stoyan, Kendall, and Mecke (1995) for detailed discussions of these models. If pdf models for the length and orientation marks are also available (cf. example in Fig. 2), a Boolean random set approach (Stoyan, Kendall, and Mecke, 1995) can be used to simulate the fractures in such a way that they are statistically compatible with the models. Hereafter, we refer to the combination of the point process model and the mark pdf models as the fracture model or fracture network model. If the fracture model is derived directly from a sample dataset, the simulation will generate fractures that resemble the data in the sense that statistics described by the model are reproduced in the simulation. Provided the fracture model adequately characterises the random features of the fracture set, a large number of simulations can be used to analyse the statistical properties related to the flow characteristics (e.g., connectivity index) of the area (volume) described by the model.

Fracture samplings, such as mapping of exposed faces in two-dimensional cases (see the example in Fig. 2) or fracture mapping of core samples, are in general exhaustive with respect to the sample area (volume). Models constructed from these types of samples are used to simulate fractures at other locations within the field where, in general, no samples are available provided the fracture random set is adequately described by the models. For this reason, unconditional simulation is normally used unless the simulation area is sufficiently close to the sampled area to be conditioned by it and/or unless limited conditioning samples (e.g., from borehole logs) are available in the simulation area (volume). The work reported in this paper is confined to unconditional simulations.

In the following investigations we use two common artificial fracture models (2D) to demonstrate the concept and the evaluation of the connectivity index. These models (denoted as Examples 1 and 2) are defined by a homogeneous Poisson point process with constant point intensity, λ, and an exponential pdf for fracture length (l) with mean parameter $1/\mu$. For fracture orientation (azimuth angle θ), Example 1 has a uniform distribution within the range $[0,\pi]$ and Example 2 has a von Mises pdf with mean parameter m and concentration parameter κ. Example 2 is used to assess the effect of fracture orientations on the CI field. The choice of pdf for fracture length and orientation follows the work published by Warburton (1980), Villaescusa and Brown (1992) and Zhang and Einstein (2000). Some authors (Bour and Davy, 1997; Odling, 1997; Bonnet and others, 2001) prefer power or lognormal models for fracture length (2D) distributions. In many applications,

however, the entire spectrum of fracture lengths from the micron scale upward is relevant and the relationship between connectivity and fracture length distribution is important. We have used the exponential model in our examples because it is simpler (only one model parameter is needed) and, consequently, easier to establish a clear relationship between CI and fracture length distribution. The exponential distribution has been shown to be an adequate model for describing fracture length distribution in practice (Priest and Hudson, 1981; Villaescusa and Brown, 1992; Zhang and Einstein, 2000) and it also gives the best fit for the example dataset shown in Figure 2C within the range of lengths considered.

The area A covered by the simulated example is $A = [0, 1] \times [0, 1]$. The simulation of a fracture random set is accomplished in two simple steps: (1) A point pattern is realised from the underlying point process model (see below), an example is given in Figure 3A for which $\lambda = 200$; (2) Each point in the realisation is marked independently by the fracture length pdf and the orientation pdf. Correlations between marks and locations and between marks themselves are not considered in this investigation but they comprise an interesting research topic in their own right. The fracture set is obtained by restoring the marks to their physical domains. Figure 3B shows simulated (truncated) fractures for Example 1 with $\mu = 9$.

CONNECTIVITY INDEX EVALUATION FOR LOCATION *X*

The connectivity between two locations can be described by an indicator variable, $c_v(x, y)$, constructed by varying y while x remains fixed (Fig. 1):

$$c_v(x, y) = \begin{cases} 1 \text{ if } x_v \leftrightarrow y_v, \ \forall x_v, y_v \in R \\ 0 \qquad\qquad\quad \text{otherwise} \end{cases} \tag{4}$$

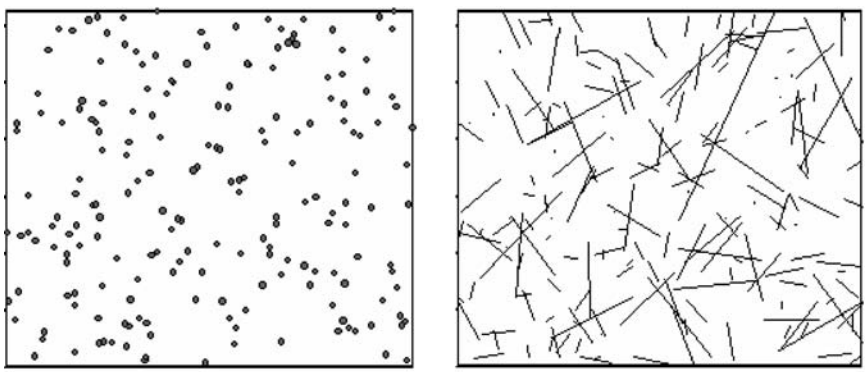

Figure 3. A, A simulated point pattern, and B, A simulated fracture set.

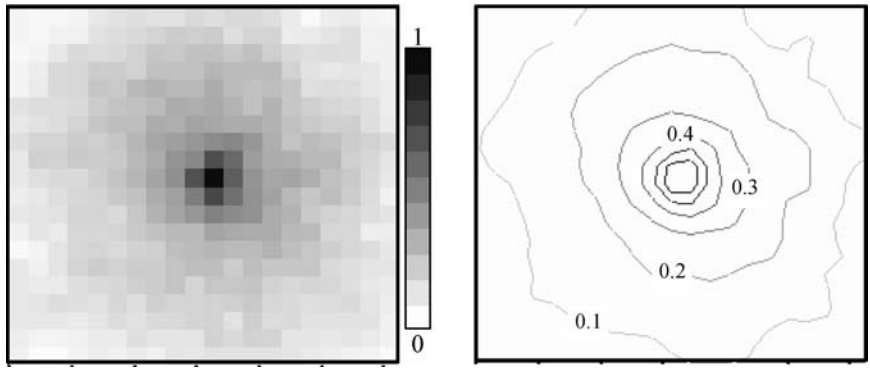

Figure 4. $\tau_v(x, y)$ for $x = (0.5,0.5)$ for Example 1 fracture model.

where $c_v(x,y)$ is a simple indicator variable that describes whether the support centred at x is connected to the support centred at y. For a specific fracture model, multiple fracture realisations can be generated using Monte Carlo (MC) simulations (see Diggle, 2003; Stoyan and Stoyan, 1994 for detailed discussion of algorithms for MC simulation of point process models). The connectivity index between locations x and y can then be calculated as:

$$\hat{\tau}_v(x, y) = \frac{1}{N} \sum_i c_v^i(x, y) \tag{5}$$

where N is the number of MC simulations and $\hat{\tau}_v$ denotes the estimator of τ_v. If y is varied to cover the region, Equation (5) describes the CI field for a fixed location x.

Figure 4 shows the CI field for location $x = (0.5,0.5)$ for Example 1 with parameters $\lambda = 200$, $\mu = 9$. Figure 5 shows the corresponding CI field at $x = (0.5, 0.5)$ for Example 2 with parameters $\lambda = 200$, $\mu = 9$, $m = \pi/4$ and $\kappa = 4.0$. The support used for both cases is $v = 0.05 \times 0.05$. A total of 100 MC simulations were used.

These two figures show the probabilities that points within the region are connected to the centre point $x = (0.5, 0.5)$, which might, for example, be the contaminant source. This probability field is important in the context of pollutant trajectories as it provides a means of quantified risk assessment of a site for a given fracture model. Some immediate observations can be made:

- $\tau_v(x, x) \equiv 1$.
- $\tau_v(x, y)$ decreases as the distance $h = |y - x|$ increases.
- variation of $\tau_v(x, y)$ is sensitive to the distribution of fracture orientations, reflecting the preferential directions of flow in the field.

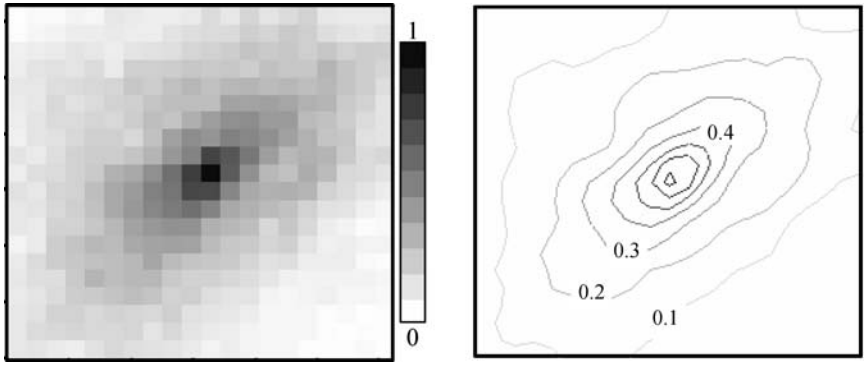

Figure 5. $\tau_v(x, y)$ for $x = (0.5,0.5)$ for Example 2 fracture model with $m = \pi/4$, $\kappa = 4$.

CONNECTIVITY INDEX FOR THE STATIONARY CASE

A more interesting case is the stationary connectivity index. The $\tau_v(x, y)$ function in Figure 4 can be expressed as $\tau_v(x, y) = \tau_v(x, |y - x|) = \tau_v(x, h)|_{h=|y-x|}$. For an underlying homogeneous Poisson point process and independent markings for both fracture lengths and orientations, this function no longer depends on the location x and $\tau_v(x, y) = \tau_v(x, h) = \tau_v(h)$ is stationary. In this case $\tau_v(h)$ yields, for a given fracture model, the probability that two points in the region, separated by a distance h, are connected. For the anisotropic case, such as that shown in Figure 5, $\tau_v(h)$ is replaced by a directional $\tau_v(h, \varphi)$ to reflect the influence of both distance and direction on the connectivity index, where φ is as shown in Figure 1.

Using MC simulations, for the isotropic case (Fig. 4), $\tau_v(h)$ can be estimated by:

$$\hat{\tau}_v(h) = \frac{1}{N|A|} \sum_i \int_A \tau_v^i(x, h)\, dx = \frac{1}{Nn} \sum_i \sum_j c_v^i(x_j, h)\, \forall x_j + h \in A \qquad (6)$$

where the indicator variable for simulation i, c_v^i, is as defined in Equation (4); n is the number of point pairs in A satisfying $x_j + h \in A$; x_j are points that provide a discrete representation of A; and N is the number of MC simulations. Because of the edge effect (discussed below) it is necessary to use multiple MC simulations to derive a reliable estimate for $\tau_v(h)$. For the anisotropic case, the direction parameter, φ, can easily be incorporated into the estimation.

The stationary connectivity indices for Examples 1 and 2 are shown in Figure 6A and Figure 6B, in which directions are measured as azimuths, i.e., the abscissa in Figures 4 and 5 has an azimuth of 90°. The figures clearly show the isotropic behaviour of the connectivity index for fractures with uniformly

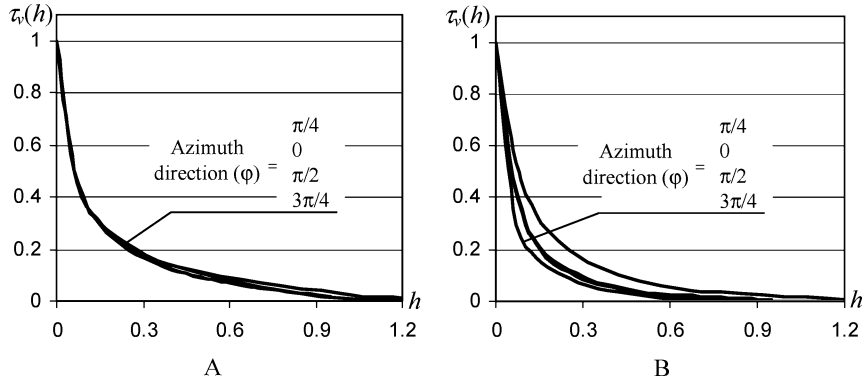

Figure 6. $\tau_v(h)$ for A, Example 1 fracture model, and B, Example 2 fracture model.

distributed orientations (Fig. 4) and the anisotropic behaviour for fractures with preferential directions (Fig. 5).

INFLUENCE OF FRACTURE MODELS ON CONNECTIVITY INDEX

Similar to percolation analysis, in which the fracture network is the decisive factor for the percolation state of the region, the fracture model also has a determining effect on the connectivity index, $\tau_v(h)$, within the field. The relationship between $\tau_v(h)$ and the fracture model parameters is important in establishing a complete connectivity function and provides vital information for sensitivity analysis and risk assessment in subsequent flow transport analysis.

In rock mass classification, fracture systems are normally quantified by indices derived from the available data. The method suggested by the International Society for Rock Mechanics (ISRM, 1978) is to use the average spacing, d_f, which is the perpendicular distance between adjacent fractures and which can also be expressed as the number of fractures per unit distance. Hestir and Long (1990) and Sahimi (1993) suggest the use of the average number of intersections per fracture, X_f, when investigating the permeability of two-dimensional fractured media using percolation theory. More recently, the fracture areal intensity parameter *P32*, termed conductive intensity, was used in the DFM analysis of the SKB project (Dershowitz and others, 1999; Outters, 2003). In two dimensions *P32* becomes *P21* which is, in fact, the intensity measure of the random closed set (fractures) (Stoyan, Kendall, and Mecke, 1995). In practice, *P32* (*P21*) can be estimated in three-dimensional cases as the average area of fractures per unit volume or, in two-dimensional cases, the average fracture length per unit area. In the work reported here the relationship between the connectivity index and X_f or *P21* is

investigated. The relationship between the connectivity index and d_f has not been investigated as the ISRM standard is designed mainly to assess the strength, not the flow properties, of rock masses in rock engineering. In two-dimensional cases, for a given set of fractures X_f and *P21* can be estimated by:

$$\begin{cases} X_f = \dfrac{1}{F}\displaystyle\sum_{i=1}^{F} x_f^i \\ P21 = \dfrac{1}{A}\displaystyle\sum_{i}^{F} L_i \end{cases} \tag{7}$$

where F is the number of fractures in the dataset and x_f^i is the number of fractures in the dataset that intersect fracture i, L_i is the length of fracture i and A is the area of the region considered.

For Example 1 fracture model, the two most important parameters are the point intensity parameter, λ, which is a measure of the number of fractures per unit area, and the size parameter μ, which is a measure of the mean fracture size (length) of the fracture set ($1/\mu$). Figures 7A–H show the connectivity index function, τ_v, for various representative λ and μ values. For these evaluations, $A = [0, 1] \times [0, 1]$ and the support $v = 0.05 \times 0.05$.

These figures clearly demonstrate that there always exists a combination of point intensity λ and average fracture length ($1/\mu$) such that it is almost certain (say with 95% confidence) that any pair of points separated by distance h are connected through the fracture network. This state is termed the percolation state (the relationship between percolation state and connectivity index is discussed further below) of the field at a scale of h and the parameters required to arrive at this state are the percolation threshold parameters (Stauffer and Aharony, 1994; Bour and Davy, 1997). Clearly, the percolation state is not solely dependent on the point intensity, λ, or the fracture length parameter, μ.

To assess the suitability of X_f and *P21* as parameters for describing fracture networks for the connectivity index, $\tau_v(h)$, shown in Figure 7 is re-plotted against the derived X_f and *P21* parameters calculated from the simulations for representative distances of $h = 0.2$, 0.4, 0.6 and 0.8 in Figure 8 and Figure 9 respectively. A least squares trend line is also fitted to the data. The cumulative squared difference between the data points and the trend line, γ, together with the correlation coefficient, ρ, between the points and the trend line are also calculated and shown in the figures and summarized in Table 1. Although there are clear indications that the $\tau_v(h)$ are functions of the X_f or *P21* parameters, the correlations between $\tau_v(h)$ and X_f are more significant than those between $\tau_v(h)$ and *P21*. There is almost a one-to-one relationship between $\tau_v(h)$ and X_f but the same can not be said for $\tau_v(h)$ and *P21*.

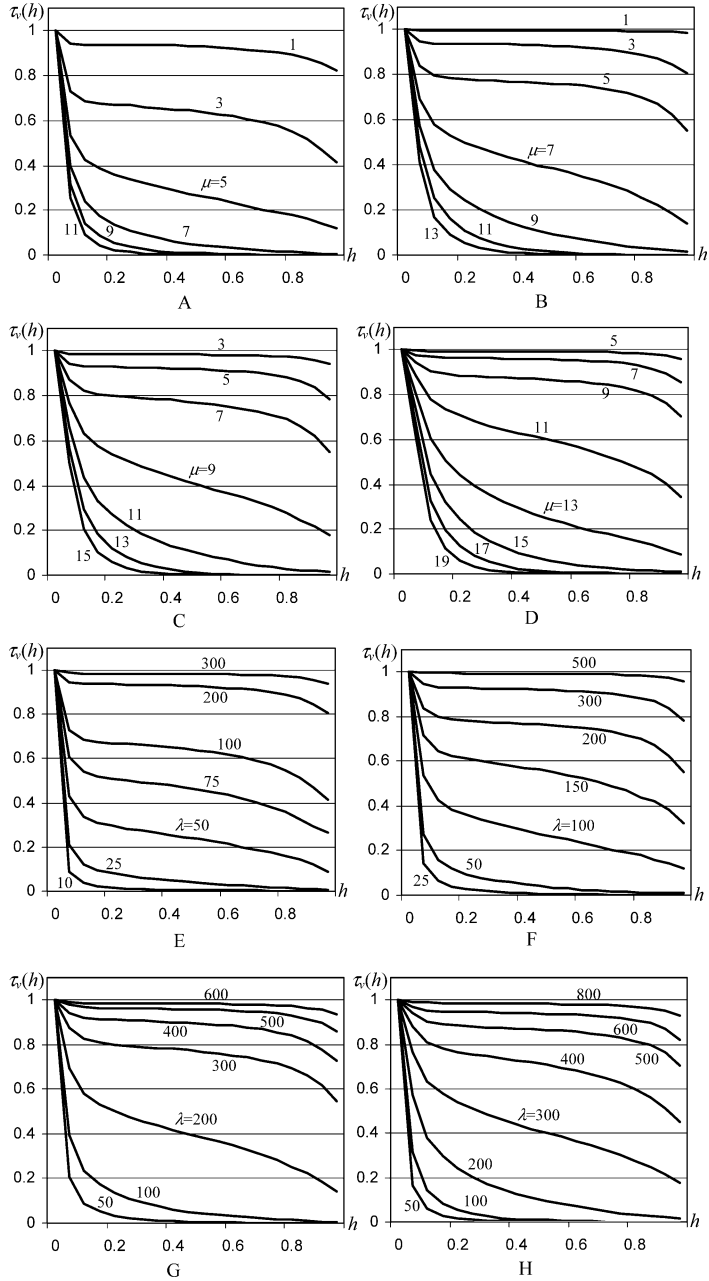

Figure 7. τ_v(h) for A, $\lambda = 100$, B, $\lambda = 200$, C, $\lambda = 300$, D, $\lambda = 500$, E, $\mu = 3$, F, $\mu = 5$, G, $\mu = 7$, and H, $\mu = 9$.

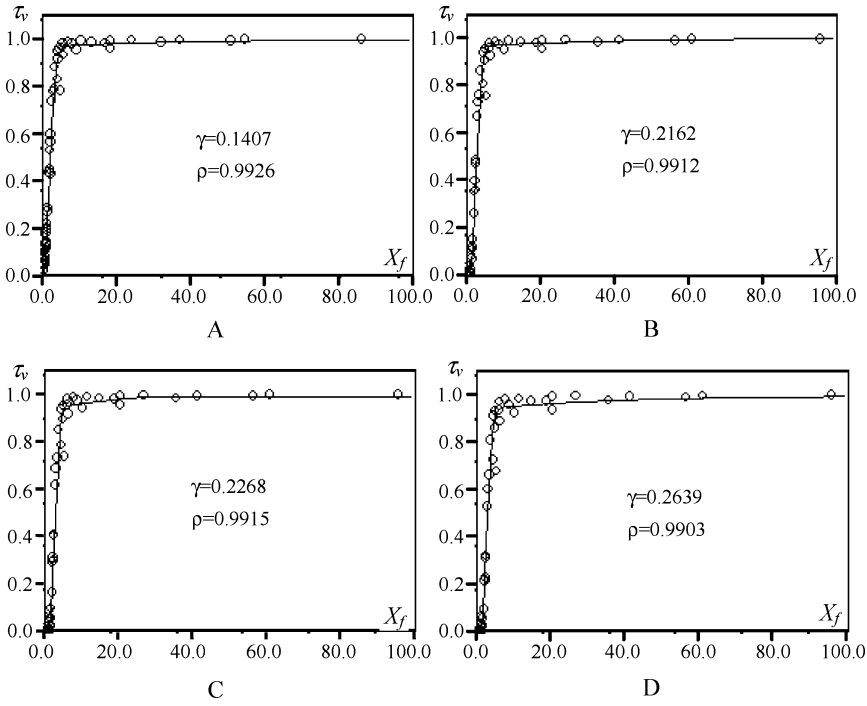

Figure 8. A, $\tau_v(0.2)$ vs X_f, B, $\tau_v(0.4)$ vs X_f, C, $\tau_v(0.6)$ vs X_f, and D, $\tau_v(0.8)$ vs X_f.

This observation demonstrates the different degrees of suitability of the parameters X_f and *P21* for describing fracture networks for the evaluation of connectivity. Further investigation reveals non-linear relationships between X_f and *P21*. For the cases considered in this paper X_f and *P21* depend only on the fracture point intensity, λ, and the fracture length parameter, μ, as shown in Figure 10A and Figure 10B (the lognormal scale is used to distinguish the curves). The relationship between X_f and *P21*, shown in Figure 11, illustrates that, firstly, their correspondence is not unique, and secondly, *P21* displays a non-linear (parabolic) trend (dependent on different values of λ and μ) against X_f. The latter observation may be partially explained by the censoring effect of fracture lines (Laslett, 1982; van Zwet, 2000) and further investigation of this effect is required.

On the basis of these observations it can be concluded that X_f is a more suitable fracture parameter than *P21* for describing fracture networks in the context of connectivity. *P21* (*P32*) may be more suitable when rock strength and stability are the main concerns, as is the case in the work conducted by Einstein (1993). In the authors' opinion, X_f (obtained experimentally or numerically) can be developed further as an effective descriptive parameter for rock mass classification for the

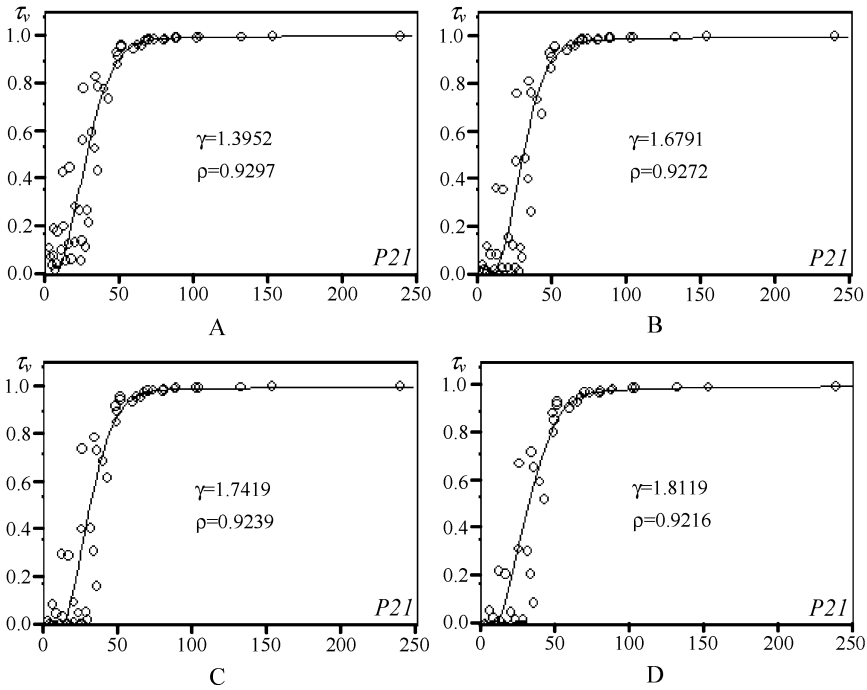

Figure 9. A, $\tau_v(0.2)$ vs *P21*, B, $\tau_v(0.4)$ vs *P2*, C, $\tau_v(0.6)$ vs *P21*, and D, $\tau_v(0.8)$ vs *P21*.

study of flow transport. Note that no attempt is made here to derive an invariant percolation threshold for the fracture network. The pros and cons of X_f and *P21* are discussed within the context of connectivity, which may have applications beyond percolation analysis. For details of invariant percolation thresholds, readers are referred to Robinson (1983), Sahimi (1993), Stauffer and Aharony (1994), and Bour and Davy (1997).

Table 1. Summary of the Correlations between the Calculated Points and the Fitted Trend Lines (Figs. 8 and 9)

	$\tau_v(h)$ vs X_f		$\tau_v(h)$ vs *P21*	
Distance h	γ	ρ	γ	ρ
0.2	0.1407	0.9926	1.3952	0.9297
0.4	0.2162	0.9912	1.6791	0.9272
0.6	0.2268	0.9915	1.7419	0.9239
0.8	0.2639	0.9903	1.8119	0.9216

γ - Accumulated squared error between the points and the trend line.
ρ - Correlation coefficients between the points and the trend line.

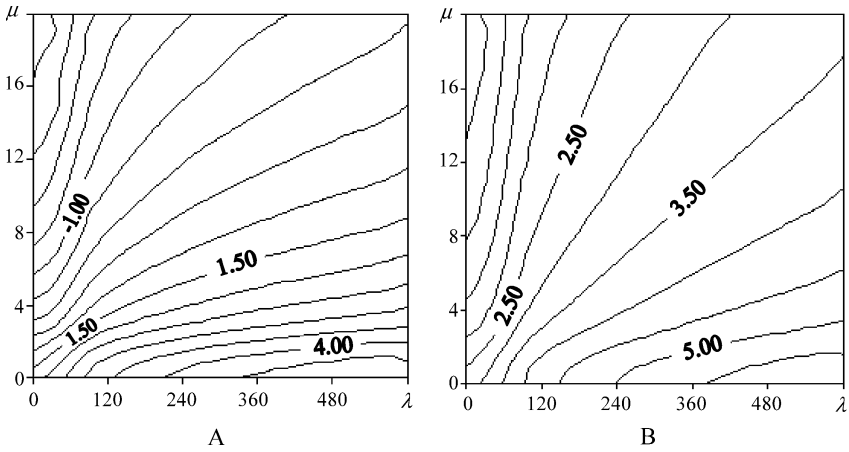

Figure 10. A, Ln (X_f) vs λ and μ; and B, Ln (*P21*) vs λ and μ.

In addition, when stationarity and isotropy can be assumed Figures 8–11 can be used to provide a quick assessment of the connectivity index of a discrete fracture model. For the example given in Figure 2, the region can be re-scaled to a square area $A = [0, 1] \times [0, 1]$. The mean fracture length after rescaling is 0.11 and the distribution is approximated by an exponential distribution with $\mu = 9$

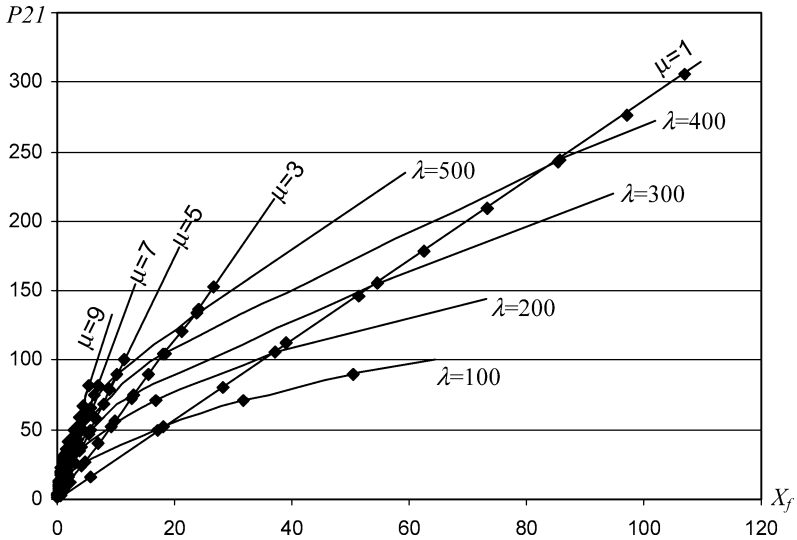

Figure 11. Relationship between *P21* and X_f.

(see Fig. 2C). With $\lambda = 426$ and ignoring anisotropy Figure 10A and Figure 10B give $X_f = 3.0$ and $P21 = 42.5$. The connectivity index of the dataset can be obtained from Figure 7H. It is not difficult to conclude that for a fracture pattern similar to that shown in Figure 2A, there is greater than 70% probability that the percolation state will be reached over the entire area.

Note that the above connectivity analysis is based on isotropic assumptions (see Fig. 4). Although details are not given here the same procedures can be used without difficulty for the anisotropic model (Example 2 fracture model).

EDGE CORRECTION, SUPPORT AND PERCOLATION ISSUES

Edge Correction

As the discrete fracture model is generated by a marked point process, edge effects may lead to biased estimates. The edge effect arises from using a limited region, R, to calculate the function, thereby excluding the influence of possible points (fractures) immediately outside the region. An illustration for two dimensions is given in Figure 12A, in which the possible connection between location x_1 and location y_3 is excluded from the evaluation of $\hat{\tau}_v(x_1, h)$ and the evaluation includes only cases in which all locations concerned (such as y_1) are within the region. Edge-corrected estimates take the influence of neighbouring regions into account and are thus unbiased. A number of edge correction procedures are available for various functions. Two popular approaches are Ripley's edge correction factor, w_{ij}, (Ripley, 1977; Diggle, 2003) and the guard area method (Ripley, 1977). The latter approach is adopted here.

In two-dimensional cases, let $A \Theta D$ denote the region A' which is the result of subtracting from region A a guard area of width D measured from the boundary of A (Fig. 12B). If $\hat{\tau}_v(h)$ is estimated only from points x within the guard area A',

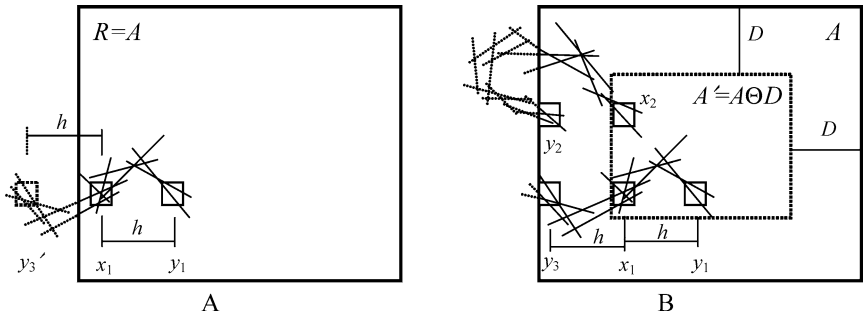

Figure 12. Edge consideration with A, no guard area, and B, guard area.

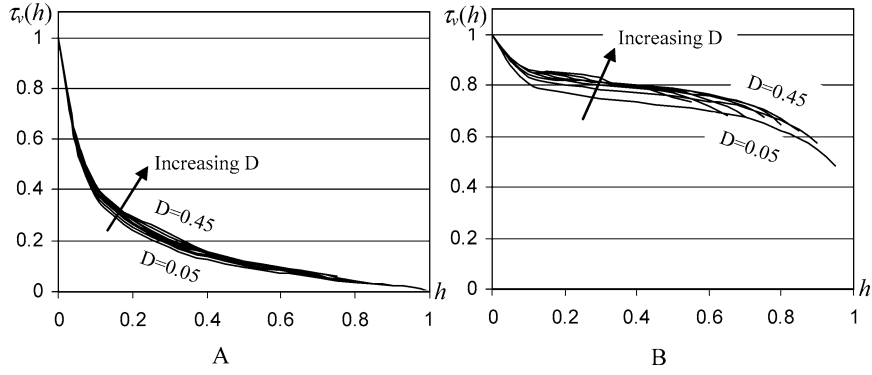

Figure 13. Edge effect for A, $\lambda = 200$, $\mu = 9$ and B, $\lambda = 400$, $\mu = 9$.

the influence of possible points (fractures) outside region A can be ignored, i.e.,

$$\hat{\tau}_v(h) = \frac{1}{N \cdot n} \sum_i \sum_j c_v^i(x_j, h) \, \forall x_j \in A' \text{ where } A' = A \Theta D \tag{8}$$

and n is now the number of point pairs in A'. This simple approach discards a large number of fractures when calculating the connectivity index.

The impact of the edge effect on the connectivity index can be assessed by varying the width, D, of the guard area. Figure 13A and Figure 13B show two $\hat{\tau}_v(h)$ functions for ($\lambda = 200$, $\mu = 9$) and ($\lambda = 400$, $\mu = 9$) with a support of $v = 0.05 \times 0.05$ respectively for different D values. As expected, $\hat{\tau}_v(h)$ increases when D increases, which reflects the inclusion of a more complete fracture network.

The increase in $\hat{\tau}_v(h)$ as D increases does not appear to be bounded. This is because of the nature of the discrete fracture network and the connectivity index function defined. Unlike a point process, for a discrete fracture network there is always a possibility that important information is excluded from the calculation no matter how small the guard area A'. For example, the possible connection network between points x_2 and y_2, shown in Figure 12B is ignored in the calculation of $\tau_v(h)$. However, compared with the impact of other fracture parameters and the support sizes (see below), the global impact of the edge correction for $\hat{\tau}_v(h)$ is insignificant.

Support

The size of the support, v, is a major determining parameter for $\tau_v(h)$. The effect of v on $\tau_v(h)$ can be seen in Figure 14 in which $\tau_v(h)$ is calculated using

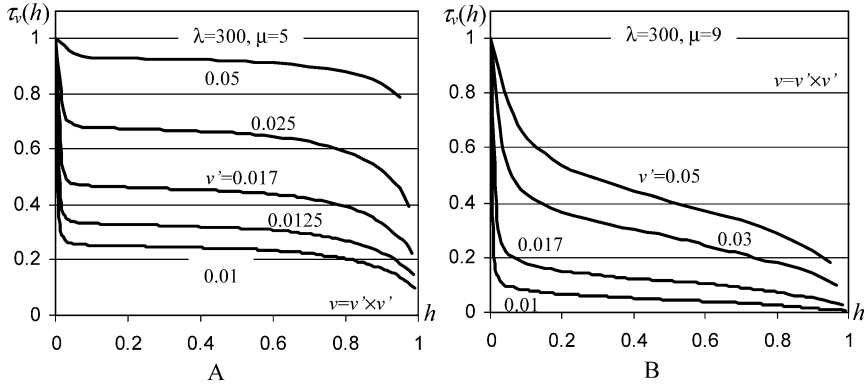

Figure 14. $\tau_v(h)$ with different supports for A, $\lambda = 300$, $\mu = 5$, and B, $\lambda = 300$, $\mu = 9$.

different supports v ranging from 0.01 (grid size of 100×100) to 0.05 (grid size of 20×20) for the area $A = [0, 1] \times [0, 1]$.

Although the choice of v is important for the evaluation of connectivity, it is a design issue. The choice depends on the appropriate scale for describing the *in-situ* flow characteristics of the rock and the nature of the flow transport problem. For example, the dissipation property of *in-situ* fractures can be used as one of the factors for deriving a suitable support scale. Another factor in support selection is the accuracy resolution required by the application to describe the CI field. The larger the support size, the more uniform is the CI field as the influence of a point on a fracture has been artificially extended to the whole support and therefore the calculated CI will be more smoothed, i.e., increased proportionally with support size. Consequently, the calculated $\hat{\tau}_v(x, y)$ is a less accurate representation of the true connectivity index between point x and y.

Relationship between Connectivity Index and Percolation State

Although the connectivity index does not directly define the percolation state, the two are obviously related. The CI defines a generic probability field for the set of fractures, which can be used in various ways. Percolation characteristics of a fractured medium can be derived from the CI by considering the percolation criteria and the system size. The fractured medium is always limited to a certain shape (e.g. rectangle in 2D) whereas the percolation state corresponds to an "infinite" fracture cluster spanning the whole system connecting either two sides or n sides of the medium boundary, i.e., two-sided (two-faced) or n-sided (n-faced) percolation (Reynolds, Stanley, and Klein, 1980; Robinson, 1984; Bour and Davy, 1997). For example, in 2D and a rectangular region, 2, 3 and 4-sided percolations can

be defined. The percolation states thus defined will, in general, yield different percolation thresholds although similar results are observed (Reynolds, Stanley, and Klein, 1980).

If the connectivity index is known for a fracture model, the probability that two sides of the boundary, say S_1 and S_2, of the region considered are connected can be evaluated as:

$$T(S_1, S_2) = T(S_2, S_1) = \sum_{S_1} \sum_{S_2} \tau(x_{S_1}, y_{S_2}) \tag{9}$$

where x_{S_1} and y_{S_2} are location points describing S_1 and S_2 independently. The probability of connection for three sides, S_1, S_2 and S_3 is:

$$\sum_{i=1}^{3} \prod_{j=1}^{2} T(S_i, S_{(i+j)\%3}) - 2 \prod_{i=1}^{3} T(S_i, S_{(i+1)\%3}), \text{ where } \% \text{ means modulo division} \tag{10}$$

And so on for the probability of an n-sided connection. It is then possible to apply a probability threshold (e.g., 0.95) and conclude that the system is at percolation state when the calculated probability exceeds the threshold. Calculations of percolation threshold parameters can then follow. The calculation of percolation probability from the CI simplifies if the underlying random fracture set is stationary.

This brief discussion covers the major relationship between CI and percolation. More work is required to describe this relationship quantitatively for various fracture models. It would be particularly interesting to investigate the CI field for the fracture network at, and around, the percolation state for different models.

CONNECTIVITY INDEX EVALUATION OF THE PRACTICAL EXAMPLE

As a practical example of CI evaluation and application, we briefly present some results for the practical example shown in Figure 2. The underlying point process is modelled by a homogeneous Poisson process with $\lambda = 426$. The model gives satisfactory summary statistics test results for the $H(t)$, $G(t)$ and $K(t)$ functions (Diggle, 2003). After rescaling, the fracture length is modelled by an exponential pdf with $\mu = 9$ and fracture orientations are represented by a non-parametric model with three main sets of fractures grouped around azimuth angles of 20°, 81° and 152° respectively. Stationarity is assumed.

Figure 15 shows the calculated results for nine directional connectivity indices $\tau_v(h, \varphi)$ for φ=0°–180°. The omni-directional CI and the CI assuming an isotropic model are also given for comparison. The same fracture pattern is subjected to

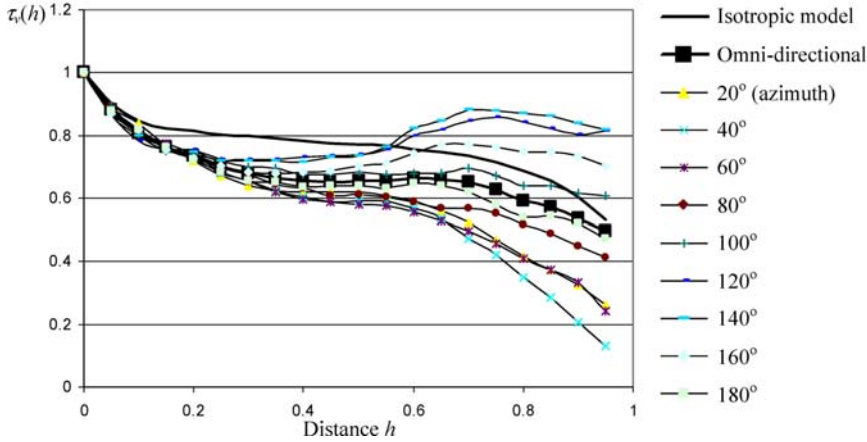

Figure 15. $\tau_v(h)$ evaluation for the example dataset.

flow simulation using the commercial package, PERFLO, which uses the finite difference, discrete fracture flow model (Odling, 2005). The average directional permeability generated by the simulations is shown in Figure 16A. To compare the CI evaluation results of the dataset with the flow simulation results, we re-plot the directional connectivity index functions shown in Figure 15 for the distance $h = 0.9$, which is approximately the size range used in the PERFLO simulation as the fracture pattern has to be rotated during the flow simulation. The result is shown in Figure 16B, which suggests that the preferential flow direction is at

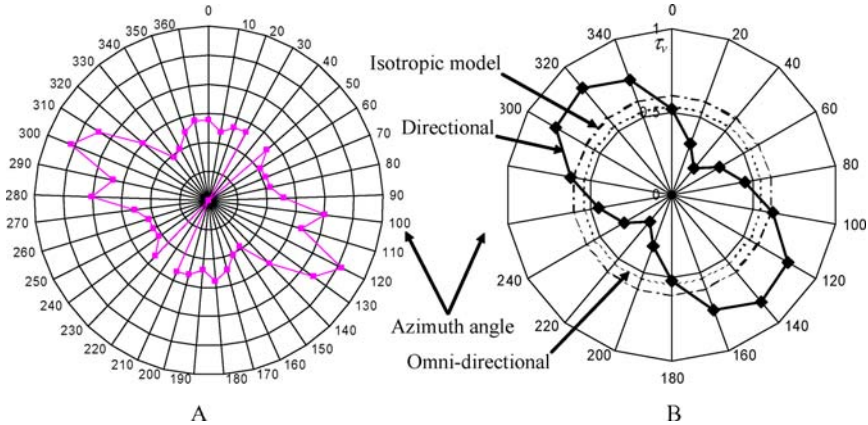

Figure 16. A, Directional permeability based on direct flow simulation, and B, Connectivity index for distance $h = 0.9$, $\tau_v(0.9)$.

an azimuth angle of 140°. At an azimuth angle of 40°, the connectivity index is around 0.2, indicating a very small chance that fractures are connected in this direction at a distance of 0.9, and hence very low permeability should be expected in this direction. These conclusions compare remarkably well with the flow simulation results in which the predicted preferential flow direction is at an azimuth angle of 120° and zero permeability is at an azimuth angle of 40°. The locus patterns of the connectivity index and the directional permeability also show remarkable similarity. It is also interesting to note that these conclusions appear to be contradictory to direct observation of Figure 2A, from which it could easily be concluded that the preferential flow direction is at an azimuth angle of 80° as most of the fractures are oriented in that direction (Fig. 2D).

CONCLUSIONS AND FUTURE RESEARCH

The connectivity index introduced in this paper describes possible point connections for the investigation of flow transport through fracture systems in rock. The index is based on a discrete fracture model which can be represented by a marked point process. The following conclusions can be drawn from the work presented here:

1. The connectivity index provides an effective means of describing the possible connections through fracture networks between a pair of points in a rock mass.
2. The connectivity index depends predominantly on three parameters: the fracture point intensity, the lengths of fractures and the orientations of fractures. Fractures can be modelled by a marked point process and the connectivity index can be evaluated by Monte Carlo simulations.
3. The connectivity index defines a generic probability field that can be used in different applications. As demonstrated, the index can be used directly for percolation evaluation and for qualitative assessment of directional permeability analysis, although more work is required to establish the quantitative relationships.
4. The average number of fracture intersections, X_f, and the fracture intensity measure, *P21* (P*32*), are two important parameters derived from the discrete fracture model. These parameters are directly related to the connectivity index and can be used to characterise rock mass properties relevant to the flow transport of pollutants. The relationship between X_f and *P21* is non-linear and the two parameters are not equivalent. X_f is more effective than *P21* in determining the connectivity index and should be used for classifying the flow characteristics of rock masses.
5. The impact of edge effects on the connectivity index is not significant when compared with the impacts of other parameters.

6. The connectivity index is sensitive to the choice of support. In practice, support selection is a design issue and an appropriate choice must be made before calculating the connectivity index.

Although we have presented only two, largely artificial, examples and have used only a two-dimensional practical example as a demonstration, the work reported can be readily extended to three dimensions and to different types of fracture models. For 3D applications, the definition and evaluation of the connectivity index remains relatively simple, but greater complexity of the fracture model is anticipated. If a marked point process is used to represent the fracture model, at least three categories of marks are required to describe size, shape and orientation of fractures. Each sub-category may require several marks depending on the complexity of the model.

ACKNOWLEDGMENT

The work reported in this paper was funded by EPSRC (Engineering and Physical Sciences Research Council) Research Grant number GR/R94602/01.

REFERENCES

Allard, D., and HERESIM Group, 1993, On the connectivity of two random set models: the truncated Gaussian and the Boolean, *in* Soares, A., ed., Geostatistics Tróia'92: Kluwer Academic Publishers, Dordrecht, The Netherlands, p. 467–478.

Allard, D., 1994, Simulating a geological lithofacies with respect to connectivity information using the truncated Gaussian model, *in* Armstrong, M., and Dowd, P. A., eds., Geostatistical simulations: Kluwer Academic Publishers, Dordrecht, The Netherlands, p. 197–211.

Bonnet, E., Bour, O., Odling, N., Davy, P., Main I., Cowie, P., and Berkowitz, B., 2001, Scaling of fracture systems in geological media: Reviews of Geophysics, v. 39, no. 3, p. 347–383.

Bour, O., and Davy, P., 1997, Connectivity of random fault networks following a power law fault length distribution: Water Resource Res., v. 33, no. 7, p. 1567–1583.

Cressie, N., 1993, Statistics for spatial data: John Wiley & Sons, New York, 900 p.

Dershowitz, B., Eiben, T., Follin, S., and Andersson, J., 1999, Alternative models project—discrete fracture network modelling for performance assessment of Aberg, technical report R-99–43, Svensk Kärnbränslehantering AB, www.skb.se.

Deutsch, C., 2002, Geostatistical reservoir modeling: Oxford University Press, Oxford, 376 p.

Diggle, P., 2003, Statistical analysis of spatial point patterns, 2nd ed.: Edward Arnold, London, 160 p.

Einstein, H. H., 1993, Modern developments in discontinuity analysis—the persistence-connectivity problem, *in* Hudson, J. A., ed., Comprehensive rock engineering: Pergamon Press, Oxford, p. 193–213.

Hestir, K., and Long, J. C. S., 1990, Analytical expressions for the permeability of random two-dimensional Poisson fracture networks based on regular lattice percolation and equivalent media theories: Jour. Geophys. Res., v. 95, B13, p. 21,565–21,581.

Hudson, J. A., and Priest, S. D., 1983, Discontinuity frequency in rock masses: Int. Jour. Rock Mech. & Mining Sci., v. 20, no. 2, p. 73– 89.

ISRM, 1978, Testing commission on standardization of laboratory and field tests. Suggested methods for the quantitative description of discontinuities in rock masses: Int. Jour. Rock Mech. & Mining Sci., v. 15, p. 319–368.

Laslett, G. M., 1982, Censoring and edge effects in areal and line transect sampling of rock joint traces: Math. Geol., v. 14, no. 2, p. 125–140.

Lee, C. H., and Farmer, I. W., 1993, Fluid flow in discontinuous rocks: Chapman & Hall, London, 169 p.

Lee, J. S., Veneziano, D., and Einstein, H. H., 1990, Hierarchical fracture trace model, *in* Hustrulid, W., and Johnson, G. A., eds., Rock mechanics contributions and challenges, proceedings of the 31st US Rock Mechanics Symposium: Balkema, Rotterdam, 1082 p.

Long, J. C. S., Remer, J. S., Wilson, C. R., and Witherspoon, P. A., 1982, Porous media equivalent for networks of discontinuous fractures: Water Resource Res., v. 18, no. 3, p. 645–658.

NRC [National Research Council], 1996, Rock fracture and fluid flow: National Academy Press, Washington, D.C., 551 p.

Odling, N., 2005, Report of flow modelling on two fracture patterns, technical report, 05/R09, Rock Deformation Group, University of Leeds, available at www.leeds.ac.uk/StochasticRockFractures.

Odling, N., 1997, Scaling and connectivity of joint systems in sandstones from western Norway: Jour. of Structural Geol., v. 19, no. 10, p. 1257–1271.

Outters, N., 2003, A generic study of discrete fracture network transport properties using FracMan/ MANFIC, technical report R-03-13, Svensk Kärnbränslehantering AB, www.skb.se.

Pardo-Igúzquiza, E., and Dowd, P. A., 2003, CONNEC3D: a computer program for connectivity analysis of 3D random set models: Computer & Geosciences, v. 29, p. 775–785.

Priest, S. D., 1993, Discontinuity analysis for rock engineering: Chapman & Hall, London, 473 p.

Priest, S. D., and Hudson, J. A., 1981, Estimation of discontinuity spacing and trace length using scanline surveys: Int. Jour. Rock Mech. & Mining Sci., v. 18, p. 183–197.

Rhén, I., and Smellie, J., 2003, Summary report—task force on modelling of ground water flow and transport of solutes. Technical Report R-03-01, Svensk Kärnbränslehantering AB, www.skb.se.

Reynolds, P. J., Stanley, H. E., and Klein, W., 1980, Large-cell Monte-Carlo renormalization group for percolation: Physical Review B, v. 21, p. 1223–1244.

Ripley, B. D., 1977, Modelling spatial patterns (with discussions): Jour. of Royal Statistical Society B, v. 39, p. 172–212.

Robinson, P. C., 1983, Connectivity of fracture systems—a percolation theory approach: Jour. of Physics A, v. 16, p. 605–614.

Robinson, P. C., 1984, Numerical calculations of critical densities for lines and planes: Jour. of Physics A, v. 17, p. 2823–2830.

Sahimi, M., 1993, Flow phenomena in rocks: from continuum models to fractals, percolation, cellular automata, and simulated annealing: Reviews of Modern Physics, v. 65, no. 4, p. 1393–1534.

Stauffer, D., and Aharony, A., 1994, Introduction to Percolation Theory, 2nd ed.: Taylor & Francis, London, 190 p.

SKB, 2003, Swedish Nuclear Fuel and Waste Management Co, http://www.skb.se.

Stoyan, D., Kendall, W., and Mecke, J., 1995, Stochastic geometry and its applications, 2nd ed.: John Wiley & Sons, New York, 436 p.

Stoyan, D., and Stoyan, H., 1994, Fractals, Random Shapes and Point Fields—Methods of geometrical statistics: John Wiley & Sons, New York, 389 p.

van Zwet, E. W., 2000, Likelihood devices in spatial statistics (in English): unpubl. doctoral dissertation, Faculteit der Wiskunde en Informatica, Universiteit Utrecht, Met samenvatting in het Nederlands, 150 p.

Villaescusa, E., and Brown, E. T., 1992, Maximum likelihood estimation of joint size from trace length measurements: Rock Mech. & Rock Eng. v. 25, p. 67–87.

Warburton, P. M., 1980, Stereological interpretation of joint trace data: influence of joint shape and implications for geological surveys: Int. Jour. Rock Mech. & Mining Sci., v. 17, p. 305–316.

Yucca Mountain, 2004, USA, http://www.nei.org.

Zhang, L., and Einstein, H. H., 2000, Estimating the intensity of rock discontinuities: Int. Jour. Rock Mech. & Mining Sci., v. 37, p. 819–837.